Can bilateral asymmetry analysis of breast MR images provide additional information for detection of breast diseases?

Ricardo J. Ferrari[1], Kimberley A. Hill[2], Donald B. Plewes[3,4], Anne L. Martel[3,4]

[1]University Health Network, University of Toronto, Toronto, ON, Canada
ricardo.jose.ferrari@gmail.com
[2]Division of Medical Oncology, Department of Medicine, Toronto, ON, Canada
[3]Imaging Research, Sunnybrook Health Sciences Centre, Toronto, ON, Canada
[4]Department of Biophysics, University of Toronto, Toronto, ON, Canada

Abstract

This paper presents a new method for bilateral asymmetry analysis of breast MR images that uses directional statistics of the breast parenchymal edges, obtained from a multiresolution local energy edge detector, and image texture information derived from local energy maps, obtained by using a bank of log-Gabor filters. Classification of MRI scans into cancer and non-cancer categories was performed by linear discriminant analysis and the leave-one-out methodology. A total of 40 cases, 20 normal/benign (BI-RADS 1 and 2) and 20 malignant, taken from a high risk screening population, were used in this pilot study. Average classification accuracy of 70% ($\kappa = 0.45 \pm 0.14$) with sensitivity and specificity of 75% and 65%, respectively, was achieved. The results obtained support the idea that bilateral asymmetry analysis of breast MR images can provide additional information for detection of breast tissue changes arising from diseases.

1 Introduction

Breast cancer is the second most common cancer among women in the world. If detected in early stages, the prognosis of this disease is very favorable with five-year survival rate exceeding 96%.

Mammography screening is still nowadays the gold standard method for early detection of breast cancer. Unfortunately, it has been shown that 10-30% of cancers are missed by this method [10]. The main reason for the missing cancers is that the cancers are often obscured by radiographically dense, fibroglandular breast tissue. Dynamic contrast-enhanced breast MRI (DCE-MRI) has shown to provide very high sensitivity with moderate specificity rates [17]. By providing 3D views, morphological and functional information (via contrast enhancement kinetics), better image contrast between breast tissue structures, large field of view, and without requiring the use of ionizing radiation, DCE-MRI has great advantages to mammography, not only in the detection but also in diagnosing and staging of the breast cancer. Despite all the benefits of DCE-MRI, it is unlikely that this imaging modality will replace mammography as a standard, widespread tool for screening of asymptomatic women. The reasons are the high cost of the exam, the limited availability and the large volume of data generated for analysis. On the other hand, DCE-MRI has been recently indicated by the American Cancer Society guideline as a screening modality for women at a "high risk" of developing breast cancer [17].

Bilateral asymmetry analysis of mammograms of a given subject is an important clinical procedure often used by radiologists to help in the diagnosis of breast cancer [2]. In the context of Computer-Aided Diagnosis (CAD) systems, bilateral asymmetry analysis may provide additional information about the presence of early signs of breast cancer that are not detected or assessed by other methods, including areas of increased density, parenchymal distortion, and small asymmetric dense regions [5, 13]. Despite the potential clinical significance of this analysis, its application to analysis of mammograms is compromised due to the tissue superposition resulting from breast compression and two-dimensional (2D) image projection, which are inherent to mammography [2] and may result in unnatural asymmetries on the images. Breast MR imaging, on the other hand, does not require breast compression, provides 3D images and presents better image contrast. Women with dense breasts, which are very difficult to diagnose via mammography, can also greatly benefit from this modality. All these facts are particularly important on this work, since women

in the high risk groups begin screening at an earlier age than the general population and therefore are more likely to have dense breasts.

In this work, we present a new method for bilateral asymmetry analysis of breast MR images, which is based on the hypothesis that breast angiogenesis will locally change the natural flow of directional structures (parenchymal edges, milk ducts, and blood vessels) oriented towards the nipple and that, by directional analysis of the linear structures present in the breast, it is possible to capture such changes. In addition, supported by the work of Warren and Lakhani [18] on the effect of breast stroma changes on the growth and progression of a breast tumor, bilateral asymmetry analysis using texture features may provide additional information to differentiate between normal and cancer cases. This paper is organized as follows. In Section 2 a brief literature review is given. Methodology and image dataset are described in Sections 3 and 4, respectively. Results and discussions are presented in Section 5 followed by the conclusions in Section 6.

2 Background

Although bilateral asymmetry analysis of breast images is an important clinical approach used by radiologists for detection of breast cancer, only a few works have been presented in the literature using this approach. Lau and Bischof [8] proposed a technique for detection of breast tumors using the asymmetry approach. The authors used the detected nipple in the image along with the pectoral chest wall as references to help in the alignment of the left and right breast images. The analysis was then performed by using a combination of four measures; brightness, roughness, brightness-to-roughness ratio, and directionality. Miller and Astley [11] have also performed comparison of corresponding anatomical regions between left and right breast images in terms of shape, texture and density. An automatic algorithm for asymmetry analysis of mammograms using morphological and directional features was proposed by Ferrari *et al*. [5, 13]. In their work, the breast extension and the pectoral muscle region were identified and removed from the left and right images. By using a breast density model, the fibroglandular disks were segmented and used for further analysis. The authors used directional statistics of linear structures and morphological and shape information extracted from the segmented fibroglandular disks in order to characterize bilateral breast asymmetries. The algorithm was applied to 88 digital mammograms and the highest classification accuracy reported was 84.4%. Alterson and Plewes [1] have presented an automatic technique for bilateral symmetry analysis of breast MRI. The technique was applied "only" to normal MRI scans of patients in the high risk group and it was demonstrated that the symmetry approach could in fact be used to match similarities between left and right breast tissues. It was suggested that this approach could consequently be used to detect bilateral changes caused by the development of a cancer. Scutt *et al.* [14] have shown evidence that breast asymmetry is higher in healthy women who are free of breast disease but subsequently go on to develop breast cancer than in women who remain disease-free in the same period. Conditional logistic regression analysis showed that, along with other established risk factors, such as family history of breast cancer and parenchymal type, breast asymmetry is an independent predictor of breast cancer. Fairly recently, Warren and Lakhani [18] have indicated that breast stroma is not inert but that there might be an interplay between the breast epithelial and stromal compartments, which have an effect on the growth and progression of a breast tumor. In this case, bilateral changes in the breast stroma may be captured by image texture analysis of the breasts.

Since a precise definition of breast asymmetry is not feasible, one could think of this term on a large range of abstraction levels. At one extreme of this range, a pixel by pixel comparison of corresponding left and right breast regions could be defined as a measure of asymmetry. However, such a definition is very naive considering the natural tissue variation between the breasts. At the other extreme, the images could be compared based on the anatomical components of the breast. In this case, image segmentation is required to determine the anatomical regions in the left and right breast images, which by itself is a very complex task. In addition, the presence of a tumor in the image can easily bias the segmentation results and description of the anatomical regions.

In the present work we use a set of features extracted from the left and right breasts to characterize changes on the breast parenchymal and image texture of MR scans. This approach is somewhere between the two extremes of abstraction, as discussed previously.

3 Methodology

Figure 1 shows a flowchart of the proposed technique. The details of the methods are described in the following sub-sections.

3.1 Image Preprocessing

Before carrying out the directional and texture asymmetry analysis, a global histogram equalization algorithm [6] was applied to the left and right MR images. The first three lowest gray levels (corresponding mostly to the image background) was not considered in the image equalization since they can largely vary from image to image. The reason for

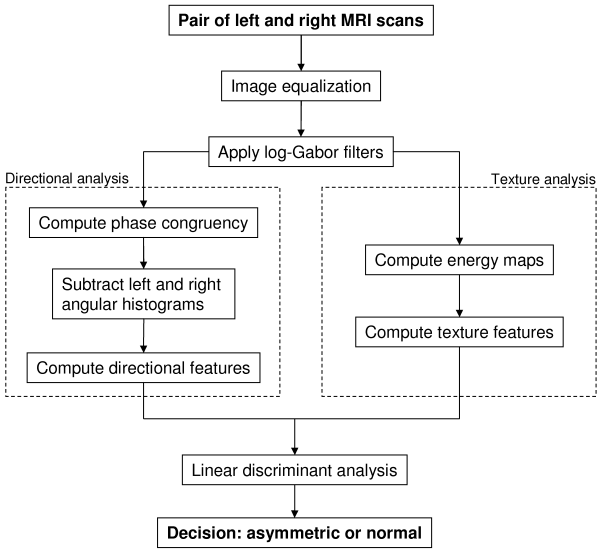

Figure 1. Flow diagram of the proposed method for bilateral asymmetry analysis of breast MR images.

this pre-processing step is twofold; first, it enhances the image contrast of the pectoral muscle region. Second, it works as an image normalization step that is also important for texture analysis.

3.2 Analysis of the parenchymal edges distribution

Assessment of global changes in the breast parenchymal, possibly caused by a developing cancer, was performed by the analysis of the parenchymal edge distribution. In this analysis, the detected edges from the left and right breasts were first mapped to their respective left and right angular histograms or rose diagrams. A rose diagram is a graphical representation of directional information [9] in which the area of each angle bin is proportional to the amount of information present in that specific direction. A set of first- and second-order directional statistics was derived from the difference between the left and right angular histograms and used for the classification. The phase congruency method [7], that is an image singularity detector based on local phase information, was used to detect the curvilinear image structures representing the parenchymal edges. In the present study, both phase and magnitude images obtained from the phase congruency method were used for the analysis.

3.2.1 Phase Congruency

The phase congruency model provides a measure of feature significance that is invariant to illumination and contrast resolution in an image [7]. PC is proportional to the local energy of a signal, which can be calculated via convolution of the original signal with a set of spatial quadrature filters [16].

For 2D images, the PC measure has been proposed in Ref. [7] as follows:

$$\mathrm{PC}_{2\mathrm{D}}(\mathbf{s}) = \frac{\sum_{n,k} W_{n,k}(\mathbf{s}) \lfloor A_{n,k}(\mathbf{s}) \Delta\Phi_{n,k}(\mathbf{s}) - T \rfloor}{\sum_{n,k} A_{n,k}(\mathbf{s}) + \epsilon}, \quad (1)$$

where $\lfloor \, \rfloor$ denotes that the enclosed quantity is equal to itself when its value is positive, and zero otherwise; $\mathbf{s}$ indicates a spatial location (x, y) in an image and $A_{n,k}(\mathbf{s})$ is the image energy at location $\mathbf{s}$, computed by using a 2D log-Gabor filter with scale n and orientation k. T is a threshold controlling the noise level of the image energy map. The term

$$W_{n,k}(\mathbf{s}) = \frac{1}{1 + \exp\left\{\gamma \left[c - \frac{1}{N}\left(\frac{\sum_n \sum_k A_{n,k}(\mathbf{s})}{A_{max}(\mathbf{s}) + \epsilon}\right)\right]\right\}}. \quad (2)$$

is a weighting function used to correct the measure from the intrinsic effect of frequency spread. The parameters γ and c in this function represent a gain factor and a cut-off value, respectively. The term $\Delta\Phi$ in Equation (1) is an energy expression used to correct for the lack of localization in the original phase congruency measure and it is defined as:

$$\begin{aligned} \Delta\Phi_{n,k}(\mathbf{s}) \quad = \quad & \cos(\phi_{n,k}(\mathbf{s}) - \overline{\phi}_{n,k}(\mathbf{s})) - \\ & \left|\sin(\phi_{n,k}(\mathbf{s}) - \overline{\phi}_{n,k}(\mathbf{s})\right| \end{aligned} \quad (3)$$

where $\overline{\phi}_{n,k}(\mathbf{s})$ is the average phase angle at position $\mathbf{s}$. The reader is referred to Ref. [7] for more details on the phase congruency model.

3.2.2 Bank of log-Gabor filters

In the present work, a bank of complex 2D log-Gabor filters was used for the implementation of the phase congruency algorithm, as described in the previous subsection. The choice for log-Gabor filters is twofold: i) log-Gabor filters have zero DC component and therefore do not respond to regions with constant gray value intensities; ii) the filters have extended tails covering high frequencies, thus making possible to obtain arbitrarily wide bandwidth.

A 1D log-Gabor function has a transfer function of the following form:

$$G(\omega) = \exp\left\{ \frac{-\left[\log\left(\frac{\omega}{\omega_0}\right)\right]^2}{2\left[\log\left(\sigma_\beta\right)\right]^2} \right\}, \quad (4)$$

where ω_0 is the central radial frequency and σ_β ($0 < \sigma_\beta < 1$) is related to the bandwidth β of the filter in octaves as

$$\sigma_\beta = \exp\left(-\frac{1}{4}\sqrt{2\log}\beta\right). \quad (5)$$

The 2D log-Gabor function is constructed in Fourier domain as the product of the 1D log-Gabor function in radial frequency, as indicated in Equation 4, and a 1D Gaussian in the angular distance, as follows

$$G(\omega,\theta) = \exp\left\{ \frac{-\left[\log\left(\frac{\omega}{\omega_0}\right)\right]^2}{2\left[\log\left(\sigma_\beta\right)\right]^2} \right\} \times \exp\left\{ -\frac{(\theta-\theta_0)^2}{2\sigma_\theta^2} \right\}, \quad (6)$$

where θ_0 is the orientation angle of the filter and σ_θ is the angular standard deviation of the Gaussian.

In practice, the real valued transfer function of the 2D log-Gabor filter given in Equation 6 is multiplied by the frequency representation of the image and, after transforming the result back to the spatial domain via inverse FFT, the results of applying the oriented energy filter pair are extracted as simply the real component for the even-symmetric filter and the imaginary component for the odd-symmetric filter. The energy and phase images are computed, respectively, as the norm and argument of the resulting complex image.

3.2.3 Design strategy of the bank of filters

The bank of filters should be designed to cover the log-frequency plane uniformly so that to achieve a fairly even spectral coverage with a minimal overlap between the filters and minimum aliasing artifacts. In other words, the transfer function of each filter should be as close as possible to a perfect bandpass filter. By appropriately setting the term σ_β, the angular standard deviation σ_θ of the angular spread Gaussian, and the number of scales S and orientations K of the bank of filters, it is possible to change the coverage of the filters.

Experimentally, we found that a very reasonable uniform spectral coverage can be obtained by fixing the maximum radial frequency center (ω_{max}) of the filters to 0.35 cycles/width and setting σ_β to 0.745, which gives filter bandwidth of one octave. In this work, the number of orientations of the bank of Gabor filters was set to 12 ($K = 12$) to allow a good angular resolution in the representation of the phase information. Since we are most interested in detecting the parenchymal edges of the breast, which correspond to high frequencies in the image, only 3 scales ($S = 3$) were used in the analysis. The central frequency of each scale is defined as $\omega_o = \omega_{max}/2^{s-1}$, with $s = 1 \ldots S$. The gain factor γ and the cut-off value c of the weighting function in Equation 2 were adjusted to 10 and 0.45, respectively, and the noise level T was set to 0.2. Experimental analysis has shown that changes on these parameters have little influence on the results of the breast parenchymal edges detection.

3.2.4 Directional statistics

After applying the phase congruency algorithm to the left and right breast MR images, a rose diagram was obtained for each breast by summarizing the phase information computed for all individual slices, as illustrated in Figures 2 and 3. In this case, one should expect that for a normal case the distribution of oriented structures in the left and right breasts will be similar, resulting in a symmetric pair of rose diagrams. Contrarily, distortion in the distribution of the natural oriented structures, possibly caused by a tumor in development, is expected to affect the symmetry between the left and right rose diagrams. A set of three directional statistical features, including preferential orientation ($\bar{\theta}$), circular variance (Var(θ)), and entropy (H) were obtained from the difference rose diagrams. The features are defined as follows:

- $\bar{\theta} = \tan^{-1}(\frac{Y}{X})$ varies from 0 to π and intends to capture the preferential orientation of the parenchymal edge flow, which for a normal breast would be normally in agreement with the straight line perpendicular to the pectoral muscle passing through the nipple.
- $\text{Var}(\theta) = 1 - \sqrt{X^2 + Y^2}$ measures the dispersion of the detected parenchymal edges. Lack of dispersion is indicated by $\text{Var}(\theta) = 0$, and maximum dispersion by $\text{Var}(\theta) = 1$.
- $H = -\sum_{i=1}^{N} R_i \log(R_i + 1.0)$ is used to represent the scatter of the parenchymal edges. The entropy value will be maximum if the parenchymal edges distribution is uniform and very small if the distribution is oriented in a very narrow angle band,

where $X = \sum_{i=1}^{N} R_i \cos\theta_i$ and $Y = \sum_{i=1}^{N} R_i \sin\theta_i$; R_i and θ_i are, respectively, the value and the central angle of the i^{th} angle band of the difference rose diagrams. In the present work, $N = 12$ is the number of bins in the rose diagrams.

In addition to the directional features obtained from the rose diagrams, a distance metric, defined as

$$D_{R,L} = \sqrt{(\mu_R - \mu_L)^2 + (\sigma_R - \sigma_L)^2}$$

was used to determine the similarity between the amount of breast parenchymal edges present on the left and right breasts. μ_R, μ_L and σ_R, σ_L are, respectively, the mean and standard deviation values of the magnitude of the phase congruency map for the right and left breast MR volumes.

3.3 Texture Analysis

Texture characterization was performed by using local energy maps computed from the complex images resulting from the convolution of a bank of log-Gabor filters with the original image. In this work, the same bank of filters used for the implementation of the phase congruency was used for texture analysis. The reasons for using local energy maps for texture analysis in this work are to minimize the processing time required in the analysis, since the same filters are used for both purposes - texture analysis and edge detection, and also because this approach is robust to image noise and intensity inhomogeneities commonly present in MR images.

Similarly to the phase congruency algorithm, the energy map $E(\mathbf{s})$ was computed for each 2D MRI slice as the magnitude of the complex filtered coefficients. The mean and standard deviation measures of each energy map were stored in four vectors ($\boldsymbol{\mu}_R$, $\boldsymbol{\mu}_L$ and $\boldsymbol{\sigma}_R$, $\boldsymbol{\sigma}_L$, respectively) for posterior analysis.

The Morgera's covariance complexity (η) [12] was used to measure changes in the texture patterns between the left and right breasts. In this measure, the squared matrix $\Gamma = (\boldsymbol{\mu}_L - \boldsymbol{\sigma}_L)(\boldsymbol{\mu}_R - \boldsymbol{\sigma}_R)^T$ was first calculated. Then, the singular value decomposition method was used to compute the eigenvalues λ_i, $i = 1, \ldots, M$, where M is the size of the feature vector. Finally, the Morgera's covariance complexity was computed as

$$\eta = -\frac{1}{\log M} \sum_{i=1}^{M} \bar{\sigma}_i \log \bar{\sigma}_i, \tag{7}$$

where

$$\bar{\sigma}_i = \frac{\lambda_i^2}{\sum_{j=1}^{M} \lambda_j^2} \tag{8}$$

is the normalized variance along the i^{th} component. The value of η lies in the closed interval $(0 \leq \eta \leq 1)$ and is inversely proportional to the correlation in the given data.

In addition, the Kullback-Leibler distance (KLD) [4] between the corresponding left and right mean and standard deviation texture feature vectors, computed as

$$KLD = \sum (\boldsymbol{\mu}_L - \boldsymbol{\sigma}_L) \log_2 \left[\frac{(\boldsymbol{\mu}_L - \boldsymbol{\sigma}_L)}{(\boldsymbol{\mu}_R - \boldsymbol{\sigma}_R)} \right] \tag{9}$$

was also used as a feature for the classification.

3.4 Pattern Recognition

Classification of the images into cancer and non-cancer classes using directional statistical and texture features was performed using linear discriminant analysis and the leave-one-out methodology, implemented in the SPSS statistical package [15]. The prior probability of each class (normal/benign and cancer) was set to 50%. Due to the limited number of samples, a pooled within-groups covariance matrix, obtained by averaging the separate covariance matrices, was used in the classification. For the same reason, an exhaustive combination of features, with permutations of up to 3 features, was used to select the best set of features for the classification.

3.5 Evaluation criteria

In the present work, the classification results were assessed by using the cross-validation average accuracy (AC), sensitivity ($Sens$), and specificity ($Spec$) measures. Kappa coefficient (κ) [3], which is a measure of scorer reliability, along with its standard error se(κ) were used to quantify the level of agreement of the cross-validation classification. κ ranges from -1 to 1, and in general, κ = 0 to 0.20 is considered slight agreement, 0.21 to 0.40 fair agreement, 0.41 to 0.60 moderate agreement, 0.61 to 0.80 substantial, and 0.81 to 1.0 outstanding. A negative kappa would indicate agreement worse than that expected by chance. se(κ) is the standard error.

4 Image Dataset

A total of 40 cases, 20 benign and 20 malignant, from patients who had previously obtained bilateral breast MRI were randomly selected from a screening population of high-risk women [17] and used in this pilot study. The study consisted of bilateral T1-weighted sagital images acquired from a 1.5T Signa GE scanner with 28 slices of 256×256 pixels resulting in an in-plane resolution of approximately 0.7mm and slice separation of 2-3mm. The images used in this analysis were obtained prior to contrast enhancement by Gd-DTPA. All the MRI scans were acquired in the middle of the menstrual cycle to avoid hormonal influences on the symmetry of the breasts. The cancer and non-cancer subject population are briefly described as follows:

- Non-cancer population: It is characterized by subjects with normal breasts and with benign findings, classified by using the Breast Imaging Reporting and Data System (BI-RADS) as categories 1 or 2, with a minimum of 2 years follow-up. The average age and menarche for the subjects on this group were 43 and 12 years, respectively. Nine women were in pre- and eleven in post-menopausal period.

- Cancer population: Twenty cases were used in this study. Table 1 shows a stratification of the cases based on the type of finding. The average cancer size of the nine invasive cancers as a subset of the twenty cancers was 0.7 ± 0.4 cm. The average age and menarche for the subjects on this group were 51 and 13 years, respectively.

Type of finding	Num.cases : (%)
Ductal Carcinoma in situ (DCIS)	8 : 40%
DCIS + microcalcifications	3 : 15%
Invasive Ductal Carcinoma (IDC)	6 : 30%
DCIS + IDC	2 : 10%
Invasive Lobular Carcinoma (ILC)	1 : 5%

Table 1. Malignant cases stratified by the type of finding.

5 Results and Discussions

Figures 2 and 3 show a benign and malignant MRI cases used to illustrate the proposed method for asymmetry analysis using directional information extracted from the distribution of the parenchymal edges. As shown in subplots (c) and (d), the phase congruency algorithm can detect very precisely most of the relevant curvilinear structures in the breast images and it is not sensitive to the MR image noise and intensity inhomogeneities.

By visually inspecting the magnitude and phase images in Figure 2, one can easily see that the parenchymal edges in the left and right images appear very similar. In this case, the left and right rose diagrams present a very good similarity in the preferential orientation of the bins. Although image processing methods using bilateral subtraction of pixel values in corresponding locations on both sides would probably fail in this case, the proposed analysis based on mapping the curvilinear edges structures of the left and right breast images to their corresponding rose diagrams seems to be able to capture the overall similarity between the breasts.

The results of the analysis of the parenchymal edges distribution for a malignant case are illustrated in Figure 3. Unlike the normal case presented in Figure 2, it is readily seen that the rose diagrams do neither present the same dominant orientation nor the same overall angular distribution. In this case, the patient was diagnosed with Ductal Carcinoma in situ and Invasive Ductal Carcinoma after a breast biopsy. The tumor was located at the upper outer quadrant of the left breast MR scan.

An important point to be noticed is that the rose diagrams illustrated in Figures 2 and 3 map the detected curvilinear structures of all slices of the respective MR volume and not just the slices presented in these figures. It should also be noticed that a slice-by-slice comparison of the rose diagrams would require registration of the left and right breast images. All the features used in the classification are normalized to account for difference in breast sizes and thus to avoid introducing bias to the results.

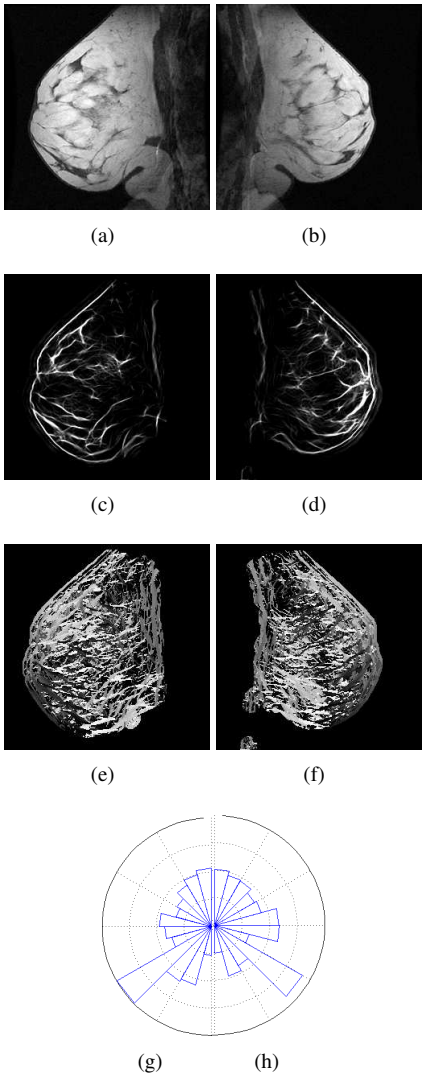

Figure 2. Benign MRI case. (a)-(b) original left and right images after histogram equalization. (c)-(d) and (e)-(f) are the magnitude and phase images resulting from the phase congruency algorithm applied to (a)-(b), respectively. (g)-(h) rose diagrams obtained from the magnitude and phase images.

A summary of the best average cross-validation results for the classification is presented in Table 2. The best av-

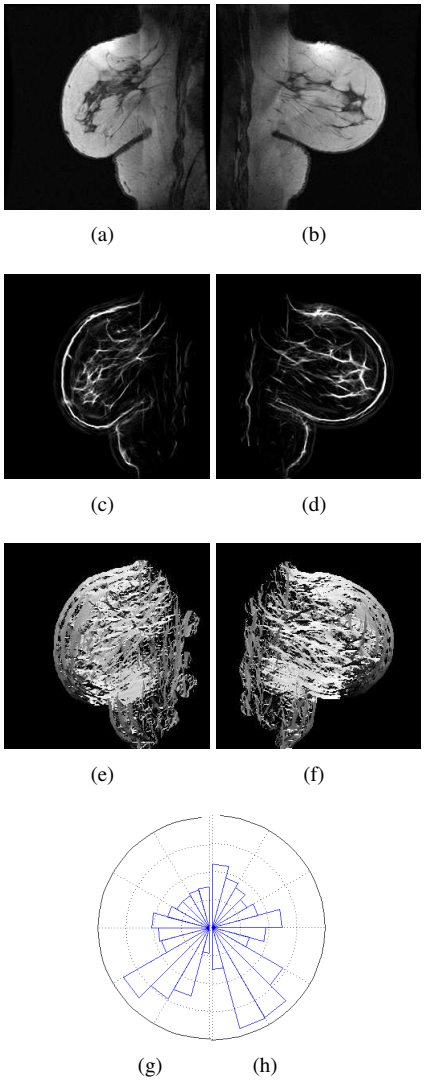

Figure 3. Malignant MRI case. (a)-(b) original left and right images after histogram equalization. (c)-(d) and (e)-(f) are the magnitude and phase images resulting from the phase congruency algorithm applied to (a)-(b), respectively. (g)-(h) rose diagrams obtained from the magnitude and phase images.

erage accuracy result achieved in this study was 72.5%, obtained by using the Morgera's covariance complexity (η) feature. The highest sensitivity rate (95%) was also achieved by using the same feature. However, in this case the specificity rate was only 50%, which means that half of the normal/benign cases were incorrectly classified. The best result by using only directional statistical features was achieved by using the similarity distance $D_{R,L}$ feature, with average accuracy of 65% and sensitivity and specificity of 50% and 80%, respectively. Texture features have shown to provide better sensitivity rates (95% for η), while directional features were more effective in classifying correctly the normal cases (specificity rate of 75% for the pair $\bar{\theta}$ and Var(θ)). Different combinations of three features have provided the best tradeoff between sensitivity (65% and 75%) and specificity (75% and 65%, respectively). The best average accuracy results presented in Table 2 have shown moderate reliability ($\kappa = 0.40$ and $\kappa = 0.45$), as indicated by the kappa coefficients.

Although, in this pilot study the method was applied to a relatively small number of cases (40 cases, 20 normal and 20 malignant), the results are encouraging, considering the small number of features used in the classification and the small size of the lesions present on the images. In fact, 55% of the malignant cases analyzed in this study are DCIS cases and the average size of the invasive tumors is 0.7 cm. In addition, the reported results were obtained by only using normal MR images, that is, no MR contrast enhancement images were used.

One important strenght of the proposed method is that it does not require any procedure for the registration or alignment of the MR scans. Because in breast MRI the patient is placed in prone position in the breast coil for the image acquisition, the gravity helps in orienting the patient breasts uniformly and therefore no alignment of the directional data related to the rose diagrams is required.

Features	Sens.	Spec.	AC	$\kappa \pm$ se(κ)
η	95%	50%	72.5%	0.45 ± 0.13
$D_{R,L}$	50%	80%	65%	0.30 ± 0.14
$\bar{\theta}$,Var(θ)	65%	75%	70%	0.40 ± 0.14
$\bar{\theta}$,$D_{R,L}$	55%	75%	65%	0.40 ± 0.14
Var(θ),$D_{R,L}$	60%	70%	65%	0.35 ± 0.15
Var(θ),η	60%	70%	65%	0.35 ± 0.15
H,η	80%	50%	65%	0.35 ± 0.14
η,KLD	90%	40%	65%	0.45 ± 0.13
$\bar{\theta}$,Var(θ),$D_{R,L}$	65%	75%	70%	0.40 ± 0.14
Var(θ),H,η	75%	65%	70%	0.45 ± 0.14

Table 2. Summary of the best average cross-validation results for the classification of the normal/benign and cancer cases.

Filtering an entire MR volume (28 slices, matrix of 256×256 pixels) with the designed bank of log-Gabor filters (3 scales and 12 orientations) takes approximately 2min on a dual-core 2GHz PC computer with 4GB of memory.

Although the technique proposed in this work shares similarities to the method in Refs. [5, 13], four main differences should be noticed; first the new proposed technique uses the phase congruency algorithm to more precisely de-

tect the most relevant curvilinear structures in an image. Second, the method uses a bank of log-Gabor filters which has the designed advantage of having zero-DC components and can be used to construct filters with an arbitrary bandwidth, and consequently can be better optimized to produce filters with minimal spatial extent. Third, the proposed technique was developed to process three dimensional images and it has been applied to detect breast cancers in MR images. Finally, the proposed technique combines directional and texture information for the image classification.

6 Conclusions

We have presented a new technique for the analysis of bilateral asymmetries in breast MR images using directional statistics of the parenchymal edges distribution and texture information. Sensitivity and Specificity values of 65 and 75%, and 75 and 65%, respectively, were achieved by using different combinations of only three features.

The method needs to be further evaluated by using a larger database and assessing the results with the receiver operating characteristic (ROC) curves. As an extension of the current work, it would be very desirable to use the temporal contrast information provided by the DCE-MRI to assess dynamic bilateral changes in the breast tissues, in addition to the static ones analyzed in this work. In this case, during the course of contrast enhancement to aid in differentiating normal from abnormal tissues, it would be expected that tumors enhance in a non-symmetric manner while normal tissues would be expected to exhibit a symmetric uptake. Other possible applications for the proposed technique are: assessment of the predisposition of a patient to develop breast cancer via longitudinal study, and follow-up of suspicious regions in an image. In the last case, the asymmetry analysis would be performed between an old MR scan, used as a reference, and a new acquired scan.

In conclusion, although the results obtained from the proposed method are insufficient to prompt biopsy, as it was already expected, they do support the idea that bilateral asymmetry analysis of breast MR images can be used as a complementary piece of information in the detection of breast tissue changes arising from disease, which is generally neglected by conventional CAD systems.

7 Acknowledgments

This study was supported by the Terry Fox Foundation and Canadian Breast Cancer Research Alliance. The authors thank Dr. Gary Wang and Dr. Elizabeth Ramsay for their assistance in provision of MR breast scans.

References

[1] R. Alterson and D. Plewes. Bilateral symmetry analysis of breast MRI. *Physics in Medicine and Biology*, 48:3431–3443, 2003.

[2] G. Cardenosa. *Breast Imaging Companion*. Lippincott-Raven, Philadelphia, NY, 1997.

[3] J. Cohen. A coefficient of agreement for nominal scales. *Educational and Psychological Measurement*, 20(1):37–46, 1960.

[4] T. Cover and J. Thomas. *Elements of Information Theory*. Wiley-Interscience, New York, NY, 1991.

[5] R. Ferrari, R. Rangayyan, J. Desautels, and A. Frère. Analysis of asymmetry in mammograms via directional filtering with Gabor wavelets. *IEEE Transactions on Medical Imaging*, 20(9):953–964, Sept. 2001.

[6] R. Gonzalez and R. Woods. *Digital Image Processing*. Addison-Wesley, Reading, MA, 1992.

[7] P. Kovesi. Phase congruency: A low-level image invariant. *Psychological Research*, 64:136–148, 2000.

[8] T. Lau and W. Bischof. Automated detection of breast tumors using the asymmetry approach. *Computers and Biomedical Research*, 24:273–295, 1991.

[9] K. Mardia. *Statistics of Directional Data*. Academic Press, New York, 1972.

[10] J. Martin, M. Moskowitz, and M. JR. Breast cancer missed by mammography. *American Journal of Roentgenology*, 132:737–739, May 1979.

[11] P. Miller and S. Astley. Automated detection of mammographic asymmetry using anatomical features. *International Journal of Pattern Recognition and Artificial Intelligence*, 7(6):1461–1476, 1993.

[12] S. Morgera. Information theoretic covariance complexity and its relation to pattern recognition. *IEEE Transactions on Systems, Man and Cybernetics*, 15(5):608–619, 1985.

[13] R. Rangayyan, R. Ferrari, and A. Frère. Analysis of bilateral asymmetry in mammograms using directional, morphological, and density features. *Journal of Electronic Imaging*, 16(1):013003/1–12, 2007.

[14] D. Scutt, G. Lancaster, and J. Manning. Breast asymmetry and predisposition to breast cancer. *Breast Cancer Research*, 8(2):1–7, Mar. 2006.

[15] S. Sweet. *Data Analysis with SPSS*. Allyn & Bacon, Boston, MA, 1999.

[16] S. Venkatesh and R. Ownes. On the classification of image features. *Pattern Recognition Letters*, 11(5):339–349, May 1990.

[17] E. Warner and et al. Surveillance of Brca1 and Brca2 mutation carriers with Magnetic Resonance Imaging, Ultrasound, Mammography, and Clinical Breast Examination. *The Journal of the American Medical Association*, 292(11):1317–1325, Sept. 2004.

[18] R. Warren and S. Lakhani. Can the stroma provide the clue to the cellular basis for mammographic density? *Breast Cancer Research*, 5(5):225–227, July 2003.